Chinese Journal of Mechanical Engineering

ORIGINAL ARTICLE

Open Access

Modified Model of Crack Tip Stress Field Considering Dislocation Slip Accumulation and Crack Tip Blunting

Jian Li[1], Bing Yang[1*], Shuancheng Wang[1], M. N. James[2,3], Shoune Xiao[1], Tao Zhu[1] and Guangwu Yang[1]

Abstract

This study uses the digital image correlation technique to measure the crack tip displacement field at various crack lengths in U71MnG rail steel, and the interpolated continuous displacement field was obtained by fitting with a back propagation (BP) neural network. The slip and stacking of dislocations affect crack initiation and growth, leading to changes in the crack tip field and the fatigue characteristics of crack growth. The Christopher-James-Patterson (CJP) model describes the elastic stress field around a growing fatigue crack that experiences plasticity-induced shielding. In the present work, this model is modified by including the effect of the dislocation field on the plastic zone of the crack tip and hence on the elastic field by introducing a plastic flow factor ρ, which represents the amount of blunting of the crack tip. The Levenberg-Marquardt (L-M) nonlinear least squares method was used to solve for the stress intensity factors. To verify the accuracy of this modified CJP model, the theoretical and experimental plastic zone errors before and after modification were compared, and the variation trends of the stress intensity factors and the plastic flow factor ρ were analysed. The results show that the CJP model, with the introduction of ρ, exhibits a good blunting trend. In the low plasticity state, the modified model can accurately describe the experimental plastic zone, and the modified stress intensity factors are more accurate, which proves the effectiveness of dislocation correction. This plastic flow correction provides a more accurate crack tip field model and improves the CJP crack growth relationship.

Keywords Digital image correlation, Back propagation neural network, Plastic zone, CJP model, Dislocation field

1 Introduction

A very large number of studies on the crack tip field have been conducted on the basis of linear elastic fracture mechanics where the stress intensity factor K is used to characterise the magnitude of the driving force causing crack growth and provide a crack growth rate relationship [1–5]. However, when the stress is greater than the yield stress in the crack-tip region, the material undergoes plastic deformation (in fact, fatigue in ductile materials is a plastic deformation-based process). Crack growth rate is therefore highly sensitive to the plastic deformation associated with crack tip deformation and growth, and the plastic zone at the crack tip and in the crack wake plays an important role in crack growth [6]. Under small-scale yielding, Irwin in 1956 [7], realised that the specimen compliance increases in the presence of plasticity, i.e., the specimen behaves as though it contains a longer crack than the actual one and also that there is a redistribution of stresses from the plastic region. Accordingly, Irwin proposed that this should be taken into account in calculating stress intensity factor (SIF) values via a plastic deformation-induced increment in crack length that should be added to the actual crack

*Correspondence:
Bing Yang
yb@swjtu.edu.cn
[1] State Key Laboratory of Traction Power, Southwest Jiaotong University, Chengdu 610031, China
[2] School of Engineering, Computing & Mathematics, University of Plymouth, Plymouth PL4 8AA, England
[3] Department of Mechanical Engineering, Nelson Mandela University, Port Elizabeth 6001, South Africa

length to calculate a modified stress intensity factor. Dugdale [8] considered the plastic zone at the crack tip in a strip yield model, that is more suited to plane stress deformation and obtained an equation for its extent that is slightly different to Irwin's model. As the crack grows, the location of the crack tip changes continuously, and the initial plastic zone at the crack tip extends with the crack to form a plastic wake, which may induce crack closure [9]. Hence, in predicting crack growth and fatigue life, it is important to accurately determine the extent and shape of the plastic zone. Budiansky and Hutchinson [10] used the Muskhelishvili potential function method based on the Dugdale model to study the influence of the crack tip plastic zone on the elastic field and proved mathematically that the plastic zone affects the elastic field of the crack tip, which leads to crack closure.

Many new test techniques, research methods and models have been proposed and applied to the study of crack tip plastic zone and its crack growth behaviour [11–13]. In 2007, Christopher et al. [14, 15] proposed the Christopher-James-Patterson (CJP) model based on Muskhelishvili complex potentials which took a new and innovative approach to characterising the effects of the plastic enclave surrounding a crack on the elastic field that drives crack growth. It was derived from many years of work by James on fatigue crack closure, and considered the possible influence of elastic-plastic compatibility stress at the elastic-plastic boundary, a dislocation-induced movement of wake material towards the crack tip [16], and plasticity-induced crack closure (modelled as an exponential decline in wake contact stress behind the crack tip). This model led to three new stress intensity factors all of which included terms arising from plasticity and which, together with the T-stress have been shown to provide an improved characterisation of the crack tip stress, strain and displacement fields in the presence of a crack growing in a plastic zone through a more accurate capture of plastic-induced shielding forces. Vasco-Olmo et al. [17] used the digital image correlation (DIC) technique to obtain the shape and size of the plastic wake that develops during crack growth. Output form the model has contributed to better understanding of the fatigue crack growth mechanisms in both constant amplitude and variable amplitude loading. As noted by Taddesse et al. [18–20], a number of authors have performed work aimed at establishing a link between fatigue life and the stress at the tip of a notch and they proposed a new model for estimating the closed-form stress at a notch tip by considering the effect of the size of the cyclic plastic zone (CPZ). This could be used for notch tip stress evaluation along the load direction and hence on crack extension from the notch. Although they claimed that their model provided a better correlation between fatigue life predictions and experimental results. However, their model did not consider the phenomenon of crack tip shielding that would be induced by the plasticity of the notch or the fatigue crack.

In the process of crack growth, dislocation formation and movement, crack blunting, cyclic hardening or softening, and crack bifurcation are all critical factors that affect crack growth rate. It is therefore necessary to quantify and separate the effect of these various factors on fatigue crack growth [21]. Dundurs and Mura [22] assessed some aspects of the interaction between the larger scale inhomogeneities and dislocations by considering an edge dislocation in the neighbourhood of a circular inclusion whose elastic properties were different from those of the surrounding matrix. Atkinson and Kanninen [23] used dislocation slip theory to simulate the plastic behaviour of a crack and revealed the hardening phenomenon of dislocation motion. Pommier [24] considered load history effects in cyclic plasticity during fatigue crack growth and pointed out that an overload causes the development of a strain gradient at the crack tip which then develops residual stresses and a reduction in the effectiveness of the subsequent fatigue cycles. Pommier and Hamam [25] assumed that the Mode-I displacement field in the near-crack tip region could be depicted by its partition into an elastic field and a plastic field. Each part of the displacement field was also assumed to be the product of a reference field, that was a function only of space coordinates a stress intensity factor. Their method provided a yield criterion and a plastic flow rule for the crack tip region that then, by assuming a relationship between plastic flow in the crack tip region and fatigue crack growth, allowed an incremental model for fatigue crack growth to be built. Hamli-Benzahar [26] studied the interaction between a dislocation and a semi-infinite crack under Mode-I loading using the finite element method. The results showed that the image forces were only generated by the presence of the dislocation and were symmetrically amplified and reduced according to the position of this dislocation with respect to the semi-infinite crack. So the orientation of the arbitrary dislocation around the semi-infinite crack generates symmetrically a positive and a negative image force which accelerate or delay the propagation of the semi-infinite crack. He et al. [27] investigated the effect of dislocations on magnesium-aluminum alloy and showed that the interaction between dislocations formed a dislocation strength zone, which hindered the development of the basal slip zone and improved the high-cycle fatigue performance of magnesium alloy. Summarising this work

on the interactions between cracks and dislocations, it is clear that their effect on crack initiation and growth and on the crack tip field is worth studying in depth.

This paper therefore proposes a new model based on the CJP crack tip field model that considers the role of dislocations in the study of the effect of crack tip fields and fatigue crack growth behaviour. The slip and stacking of dislocations affects crack initiation and growth, leading to changes in the crack tip field; it leads to material hardening behaviour and reduces plastic toughness, so that the fatigue properties of the material ahead of the crack are changed. The work was performed on the commonly used rail steel U71MnG. This steel experiences cyclic loading during service, and the surface layer is prone to dislocation hardening from wheel slip. From a micro-impact perspective, based on use of the CJP model, the influence of dislocation slip accumulation and blunting are further considered. The dislocation field is used to modify the CJP model, and a plastic flow factor ρ is introduced, thus leading to a new mathematical model for characterizing the crack tip elastic field. The results from this new model are validated and then compared with those obtained with the existing version of the CJP model. The results show that the new model has advantages for characterizing the crack tip field and crack growth behaviour.

2 Plasticity-Corrected Crack Tip Field Model

2.1 Introduction to the CJP Model

The CJP model, which is now widely studied worldwide, can better describe the plasticity-induced shielding phenomenon and elastoplastic compatibility stress than the traditional Paris relationship using Irwin SIF values. The CJP model is therefore the theoretical basis of this study [28, 29]. Christopher et al. [14] mathematically modeled several stresses that are potentially affected by the presence of the plastic zone. They combined experimental data obtained from phase-stepping photoelasticity method with a Muskhelishvili complex potential stress analysis of the forces conceptually shown in Figure 1.

When the crack opens, the plastic zone contracts in the x-direction and expands in the y-direction. The plastic wake shrinks in the x-direction. Thus, the shear force F_S is obtained according to the displacement compatibility. The forces F_{Ax} and F_{Ay} of the stress field, corresponding to the crack tip, are generated by the external load, which drives crack growth and is characterised by the stress intensity factor K_I.

When the crack closes, forces F_{Px} and F_{Py} are generated owing to the permanent deformation on both sides of the interface and the elastoplastic interaction. The plastic wake stretches in the x-direction, which produces an opposite shear force F_S owing to the coordination requirements; it expands in the y-direction, which

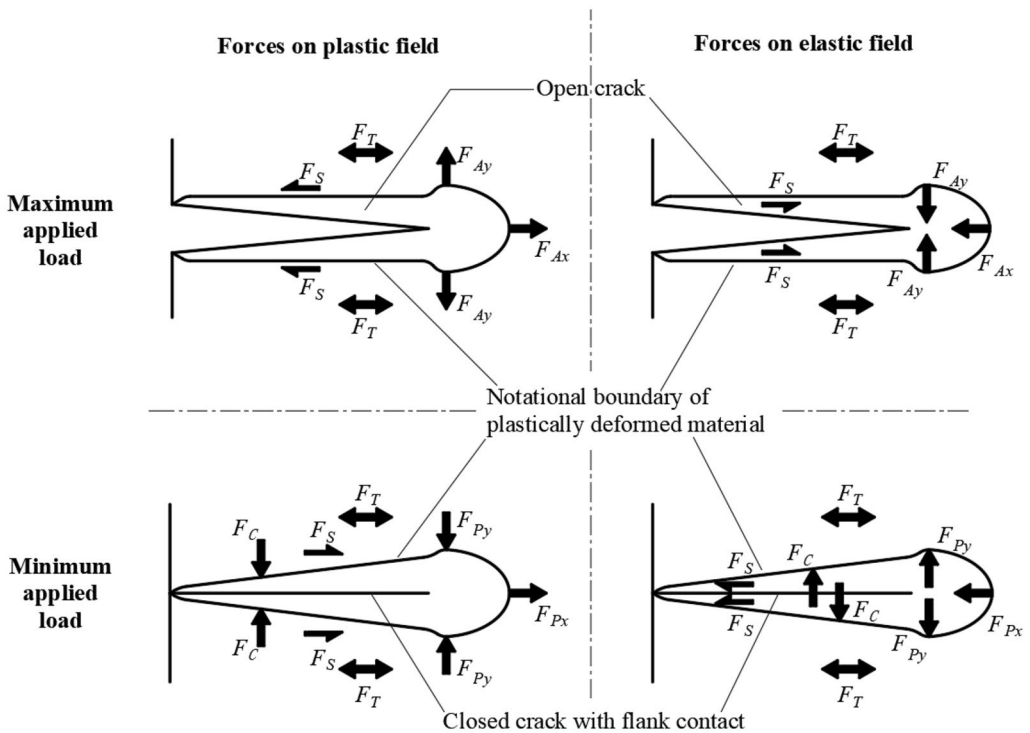

Figure 1 Schematic diagram of crack tip force in the CJP model [14]

results in a compressive contact force F_C. F_C and F_P are regarded as the forces generated by permanent plastic deformation, which hinder crack growth and result in a plastic shielding effect.

The stress field of the CJP model under Mode-I loading [14] can be expressed as:

$$\sigma_x = -\frac{1}{2}r^{-\frac{1}{2}}\left\{\begin{array}{l}(A+4B+8F)\cos\dfrac{\theta}{2}+B\cos\dfrac{5\theta}{2}\\ +F\left[\begin{array}{l}\ln r\left(\cos\dfrac{5\theta}{2}+3\cos\dfrac{\theta}{2}\right)\\ +\theta\left(\sin\dfrac{5\theta}{2}+3\sin\dfrac{\theta}{2}\right)\end{array}\right]\end{array}\right\}-C+O\left(r^{\frac{1}{2}}\right), \tag{1}$$

$$\sigma_y = \frac{1}{2}r^{-\frac{1}{2}}\left\{\begin{array}{l}(A-4B-8F)\cos\dfrac{\theta}{2}+B\cos\dfrac{5\theta}{2}\\ +F\left[\begin{array}{l}\ln r\left(\cos\dfrac{5\theta}{2}-5\cos\dfrac{\theta}{2}\right)\\ +\theta\left(\sin\dfrac{5\theta}{2}-5\sin\dfrac{\theta}{2}\right)\end{array}\right]\end{array}\right\}+O\left(r^{\frac{1}{2}}\right), \tag{2}$$

$$\sigma_{xy} = -\frac{1}{2}r^{-\frac{1}{2}}\left[\begin{array}{l}A\sin\dfrac{\theta}{2}+B\sin\dfrac{5\theta}{2}\\ +2F\left(\begin{array}{l}\ln r\sin\theta\cos\dfrac{3\theta}{2}\\ +\theta\sin\theta\sin\dfrac{3\theta}{2}\end{array}\right)\end{array}\right]+O\left(r^{\frac{1}{2}}\right), \tag{3}$$

where σ_x, σ_y, σ_{xy} represent the stresses in x, y and shear directions respectively; A, B, C, and F are the four parameters that define the crack tip field in the CJP model; r is the distance to the crack tip; and θ is the polar angle to the crack surface; in the limit $r \to 0$ near to the crack tip, the higher order term $O(r^{1/2})$ becomes negligible.

The displacement field of the CJP model under Mode-I loading [15] can be expressed as:

$$\begin{aligned}2G(u+iv) =& \kappa\left[-2(B+2F)z^{\frac{1}{2}}+4Fz^{\frac{1}{2}}-2Fz^{\frac{1}{2}}\ln(z)-\frac{C}{4}z\right]\\ &+z\left[(B+2F)\bar{z}^{-\frac{1}{2}}+F\bar{z}^{-\frac{1}{2}}\overline{\ln(z)}+\frac{C}{4}\right]\\ &-\left[A\bar{z}^{\frac{1}{2}}-F\bar{z}^{\frac{1}{2}}\overline{\ln(z)}+2F\bar{z}^{\frac{1}{2}}+\frac{C}{2}\bar{z}\right],\end{aligned} \tag{4}$$

where u and v represent horizontal and vertical displacement respectively; G is the shear modulus and $G = E/[2(1+\upsilon)]$, in which E is Young's modulus and υ is the Poisson's ratio; $\kappa = (3-\upsilon)/(1+\upsilon)$ for plane stress, and $\kappa = 3-4\upsilon$ for plane strain; z is the complex co-ordinate in the physical plane, $z = x + iy$, x and y are co-ordinates in a Cartesian system with the origin at the crack tip.

The stress intensity factor K_F, which drives crack growth, is generated by external loading. When there is no plasticity, the definition of K_F is the same as that of the traditional stress intensity factor K_I. Owing to the existence of the plastic wake and the difference in Poisson's ratio, elastoplastic compatibility stress is generated in the crack wake, which leads to the generation of shear stress intensity factor K_S along the crack side, and a stress intensity factor K_R parallel to the crack is generated to prevent crack growth due to the crack surface contact and elastoplastic compatible stress. T is T stress.

These three newly defined stress intensity factors K_F, K_R, and K_S in the CJP model of crack tip fields can be obtained as follows:

$$\begin{aligned}K_F &= \lim_{r\to 0}\sqrt{2\pi r}\left[\sigma_y + 2Fr^{-0.5}\ln r\right]\\ &= \sqrt{\frac{\pi}{2}}(A-3B-8F),\end{aligned} \tag{5}$$

$$K_S = \lim_{r\to 0}\left(\sqrt{2\pi r}\sigma_{xy}\right) = \mp\sqrt{\frac{\pi}{2}}(A+B), \tag{6}$$

$$K_R = \lim_{r\to 0}\left(\sqrt{2\pi r}\sigma_x\right) = -(2\pi)^{\frac{3}{2}}F, \tag{7}$$

$$T = -C. \tag{8}$$

This is very different from the traditional elastic model of crack tip stresses. The CJP model characterises the shielding and elastoplastic compatibility of the plastic zone, which better characterises crack growth in the presence of plasticity-induced shielding.

2.2 Derivation of Dislocation Field

When a metallic structure is deformed past the elastic limit by external forces, dislocations will move through the crystal lattice under the action of these forces while new dislocations are generated. Dislocation movement leads to slip occurring in the alloy. When dislocations encounter the barrier of the grain boundary (which is itself a dislocation array), further movement is blocked and a dislocation pile-up will form at the boundary. Further movement can only occur once the stress ahead of the pile-up reaches a level sufficient to cross the barrier. The accumulated dislocations can lead to the creation of voids and microcracks at the grain boundaries, which are the initiation sites for fatigue or fracture.

As shown in Figure 2, according to Bueckner's theorem, a planar crack opened by tensile external loading (Figure 2(a)) can be superimposed by the internal stress generated along the crack line by an uncracked object and the stress generated by a similar crack in the same object subjected to internal pressure when unloaded; as shown in Figure 2(b), the internal stress of the subject is distributed on the crack line, and as shown in Figure 2(c), the dislocation is distributed on the crack line to simulate

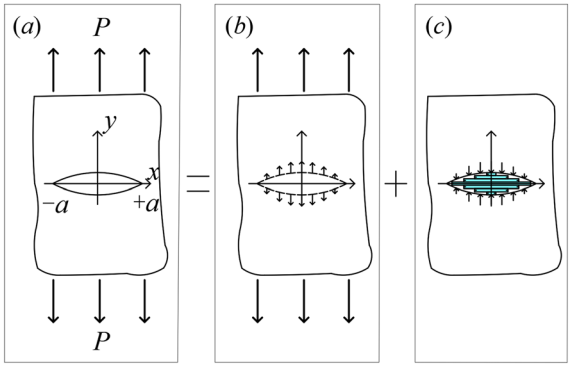

Figure 2 Crack edge dislocation based on Bueckner's theorem [31]

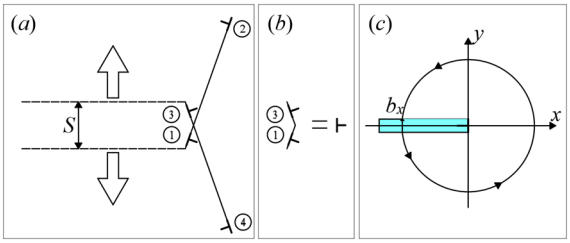

Figure 3 Edge dislocation and its dipole diagram: **a** Dislocation dipoles; **b** crack tip dislocations; **c** edge dislocation of the Mode-I crack

crack face separation. If a externally loaded continuous elastic body contains a notional cut along $x = \pm a$, $y = 0$, a traction along the crack edge can be visualised as existing. Closing this notional crack requires material to be inserted into the fracture surface gap to simulate crack surface separation that induces equal and opposite forces on the fracture surfaces. Finally, the systems are connected to form a new continuous object, which forms edge dislocations, also known as climbing dislocations [30]. Based on the continuous dislocation theory, the crack-dislocation problem can be transformed into a pure dislocation problem to study the total dislocation-induced stress field at the tip by simulating the crack and the corresponding dislocation motion with dislocations.

The dislocation strength is equal to the open gap, which is called the *Burgers* (b_x, b_y) vector. Because the Mode-I crack growth is only affected by the opening force perpendicular to the crack, there is no shear force; therefore, b_x is 0. Therefore, the Mode-I crack growth has a *Burgers* vector with dislocation strength b_y, and the corresponding dislocation field stress function [30] is:

$$\phi = \frac{2Gb_y}{\pi(\kappa+1)} r \cdot \log(r) \cdot \cos\theta. \tag{9}$$

The expression of the dislocation displacement field $\underline{u}^{\perp}$ is as follows:

$$u_x^{\rho}(r,\theta) = \frac{\rho}{\pi(\kappa+1)}\left[(\kappa-1)\ln r - 2\cos^2\theta\right], \tag{10}$$

$$u_y^{\rho}(r,\theta) = \frac{\rho}{\pi(\kappa+1)}[(\kappa+1)\theta - 2\cos\theta\sin\theta], \tag{11}$$

where ρ is the plastic flow factor caused by the dislocation field and represents the blunting of the crack tip.

The plasticity that occurs at the crack tip is illustrated in Figure 3(a) and is represented by two dislocation dipoles on the glide plane. The dislocation strength of the two dislocations in each dipole is equal to zero to maintain a constant volume during plastic deformation. The dipole produces an internal force to shield the remote load, which corresponds to the plastic shielding effect in the CJP model. The insertion of dislocations 1 and 3 as seen in Figure 3(b) is a stress source along the crack line, which causes the singularity of the crack tip field. The single edge dislocation located at the crack tip in Figure 3(c) indicates the dislocation behaviour of the Mode-I crack. Its dislocation strength is equal to the sum of the vectors of dislocations 1 and 3; however, it has opposite signs to restore the traction-free state along the crack surface and eliminate the singularity of the crack tip, which generates dislocation fields $\underline{u}^{\perp}$ [25].

Under external load, the actual displacement field $\underline{u}(\underline{x})$ consists of three parts: elastic displacement $K_I^{\infty}\underline{u}^e(\underline{x})$ caused by the range load, displacement $K_I^{sh}\underline{u}^e(\underline{x})$ caused by the internal stress formed by the plastic effect of the crack tip, and necessary geometric dislocation $\rho\underline{u}^{\perp}(\underline{x})$. Therefore, the displacement field [25] is expressed as:

$$\begin{aligned}\underline{u}(\underline{x}) &= \left(K_I^{\infty} + \delta K_I^{sh}\right)\underline{u}^e(\underline{x}) + \rho\underline{u}^{\perp}(\underline{x}) \\ &= \tilde{K}_I\underline{u}^e(\underline{x}) + \rho\underline{u}^{\perp}(\underline{x}).\end{aligned} \tag{12}$$

Considering the effect of plasticity effect produces a stress intensity factor K_I^{sh}, which is similar to the three new stress intensity factors produced by the CJP model considering the effect of plasticity-induced shielding and elastoplastic compatible stress. $\tilde{K}_I = K_I^{\infty} + K_I^{sh}$ are the same as the stress intensity factors K_F, K_R, and K_S in the CJP model. In this study, the dislocation field is used to modify the CJP model to include effects of dislocation motion and crack-tip blunting behaviour in the presence of plastic effects.

The dislocation motion satisfies the assumption of small deformation, and the dislocation stress field can be calculated from Eqs. (10) and (11) using the geometric equations in elastic mechanics combined with the generalised Hooke's law [32]:

$$\sigma_x^{\rho} = E\rho\left[\frac{(\cos\theta + \cos 3\theta)}{(4\pi r)}\right], \tag{13}$$

$$\sigma_y^{\rho} = E\rho\left[\frac{3\cos\theta - \cos 3\theta}{(4\pi r)}\right], \tag{14}$$

$$\sigma_{xy}^{\rho} = E\rho\left[\frac{(\cos 2\theta \cdot \sin\theta)}{(2\pi r)}\right]. \tag{15}$$

The two displacement field forms are both in the elastic region and satisfy the assumption of a small deformation. Based on Bueckner's theorem, the real displacement field in the region of the crack tip is obtained by superimposing Eq. (4) with Eqs. (10) and (11) respectively:

$$u^* = \left\{\begin{array}{l} \dfrac{\sqrt{r}}{2G}\left\{\begin{array}{l}(-A-2B\kappa-2F)\cos\dfrac{\theta}{2}+(B+2F)\cos\dfrac{3\theta}{2}\\ -F\left[\begin{array}{l}\ln(r)\left(\cos\dfrac{3\theta}{2}+(1-2\kappa)\cos\dfrac{\theta}{2}\right)\\ +\theta\left(\sin\dfrac{3\theta}{2}+(2\kappa-1)\sin\dfrac{\theta}{2}\right)\end{array}\right]\\ +\dfrac{C}{4}r^{0.5}(1+\kappa)\cos\theta\end{array}\right\}\\ +\dfrac{\rho}{\pi(\kappa+1)}\left[(\kappa-1)\ln r-2\cos^2\theta\right]\end{array}\right\}, \tag{16}$$

$$v^* = \left\{\begin{array}{l} \dfrac{\sqrt{r}}{2G}\left\{\begin{array}{l}(A-2B\kappa+2F)\sin\dfrac{\theta}{2}+(B+2F)\sin\dfrac{3\theta}{2}\\ +F\left[\begin{array}{l}\ln(r)\left(\sin\dfrac{3\theta}{2}-(1+2\kappa)\sin\dfrac{\theta}{2}\right)\\ -\theta\left(\cos\dfrac{3\theta}{2}+(1+2\kappa)\cos\dfrac{\theta}{2}\right)\end{array}\right]\\ +\dfrac{C}{4}r^{0.5}(3-\kappa)\sin\theta\end{array}\right\}\\ +\dfrac{\rho}{\pi(\kappa+1)}[(\kappa+1)\theta-2\cos\theta\sin\theta]\end{array}\right\}. \tag{17}$$

Correspondingly, Eqs. (13), (14), and (15) are superimposed with Eqs. (1), (2), and (3), respectively, and the actual stress field is then obtained as follows:

$$\sigma_x^* = \left\{\begin{array}{l} -\dfrac{1}{2}r^{-\frac{1}{2}}\left\{\begin{array}{l}(A+4B+8F)\cos\dfrac{\theta}{2}+B\cos\dfrac{5\theta}{2}\\ +F\left[\begin{array}{l}\ln r\left(\cos\dfrac{5\theta}{2}+3\cos\dfrac{\theta}{2}\right)\\ +\theta\left(\sin\dfrac{5\theta}{2}+3\sin\dfrac{\theta}{2}\right)\end{array}\right]\end{array}\right\}\\ -C+E\rho\left[\dfrac{(\cos\theta+\cos 3\theta)}{(4\pi r)}\right]\end{array}\right\}, \tag{18}$$

$$\sigma_y^* = \left\{\begin{array}{l} \dfrac{1}{2}r^{-\frac{1}{2}}\left\{\begin{array}{l}(A-4B-8F)\cos\dfrac{\theta}{2}+B\cos\dfrac{5\theta}{2}\\ +F\left[\begin{array}{l}\ln r\left(\cos\dfrac{5\theta}{2}-5\cos\dfrac{\theta}{2}\right)\\ +\theta\left(\sin\dfrac{5\theta}{2}-5\sin\dfrac{\theta}{2}\right)\end{array}\right]\end{array}\right\}\\ +E\rho\left[\dfrac{3\cos\theta-\cos 3\theta}{(4\pi r)}\right]\end{array}\right\}, \tag{19}$$

$$\sigma_{xy}^* = \left\{\begin{array}{l} -\dfrac{1}{2}r^{-\frac{1}{2}}\left[\begin{array}{l}A\sin\dfrac{\theta}{2}+B\sin\dfrac{5\theta}{2}\\ +2F\left(\begin{array}{l}\ln r\sin\theta\cos\dfrac{3\theta}{2}\\ +\theta\sin\theta\sin\dfrac{3\theta}{2}\end{array}\right)\end{array}\right]\\ +E\rho\left[\dfrac{(\cos 2\theta\cdot\sin\theta)}{(2\pi r)}\right]\end{array}\right\}. \tag{20}$$

The dislocation-based modification to the CJP model does not change the definition of the stress intensity factors in the CJP model, and the expression containing the term ρ of the plastic flow factor is related to r. In the present study, the stress intensity factors of the modified model were obtained based on the definition of the stress intensity factor in the CJP model, and the new expressions are obtained as follows:

$$\begin{aligned} K_{F^*} &= \lim_{r\to 0}\sqrt{2\pi r}\left[\sigma_y(r,0)+2Fr^{-0.5}\ln r-\frac{E\rho}{2\pi r}\right]\\ &= \sqrt{\frac{\pi}{2}}(A-3B-8F), \end{aligned} \tag{21}$$

$$K_{S^*} = \lim_{r\to 0}\sqrt{2\pi r}\left[\sigma_{xy}(r,\pm\pi)\right] = \mp\sqrt{\frac{\pi}{2}}(A+B), \tag{22}$$

$$K_{R^*} = \lim_{r\to 0}\sqrt{2\pi r}\left[\sigma_x(r,\pm\pi)-\frac{E\rho}{2\pi r}\right] = -(2\pi)^{\frac{3}{2}}F, \tag{23}$$

$$K_{\rho *} = \rho. \tag{24}$$

3 Experimental Techniques

3.1 Materials and Methods

The test material was U71MnG rail steel, and its mechanical properties and chemical compositions are listed in Tables 1 and 2, respectively. The fatigue crack growth experiment was performed on an ElectroPuls E3000 dynamic testing machine with the double edged-notched tensile (DENT) specimens with a thickness of 1 mm, as shown in Figure 4. The test used sinusoidal loading with a frequency of 10 Hz, maximum load of 2400 N, and stress

Table 1 Mechanical property parameters of U71MnG rail steel

E (GPa)	σ_b (MPa)	σ_s (MPa)	ε_f (%)	υ
210	≥ 880	780	≥ 10	0.28

ratio R of 0.1. A Dantec Q-400 3D digital image correlation system was used to obtain full-field data. Before the test, the first surface was polished and sprayed with a random distribution of white speckles on a black background, while the other surface was polished to track the crack-tip position using a high-magnification lens. The size of the DIC image acquisition field was 1624 × 1202 pixels, and each pixel corresponded to an actual size of 0.0114 mm.

3.2 Back Propagation (BP) Neural Network

In this part of the work, the plastic zone was related to the stress intensity and, as the area of the plastic zone is an important parameter for describing crack growth rate, it can be used as a comparison parameter for the optimisation process [33]. Carolo et al. [34] used two techniques to evaluate the shape and size of the plastic zone, and the results showed that the thermal parameter map gave effective SIF range factors that were consistent with the results obtained using the CJP model, implying that both techniques could more accurately describe the elastic stress field around the crack tip in the presence of plasticity-induced shielding. Acquiring an accurate displacement field via DIC is the key to accurate identification of the plastic zone size and shape using the CJP model. However, using DIC to calculate the original displacement field will have the influence of noise and other factors. Direct use of the displacement field will amplify the noise to a certain extent, and the strain field is not accurate. In order to overcome this problem, Pan [35] proposed a method based on the least squares principle, using the two-dimensional Savitzky-Golay (SG) full-field strain solution method to solve the strain field. This approach was adopted in the present paper. The open-source software Ncorr was used to obtain displacement cloud map data and the full-field images of lateral (x-direction) and vertical (y-direction) displacements are shown in Figure 5. Then, the stress field can be solved using the generalised Hooke's law. This solution was substituted into the von Mises yield criterion to obtain the size and shape of the experimental plastic zone.

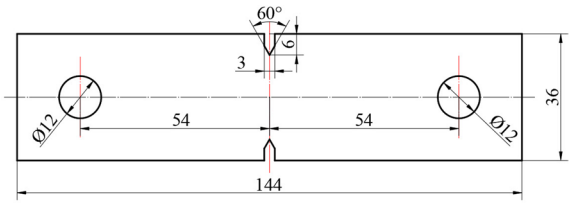

Figure 4 Dimensions of the double edge-notched specimen (unit: mm)

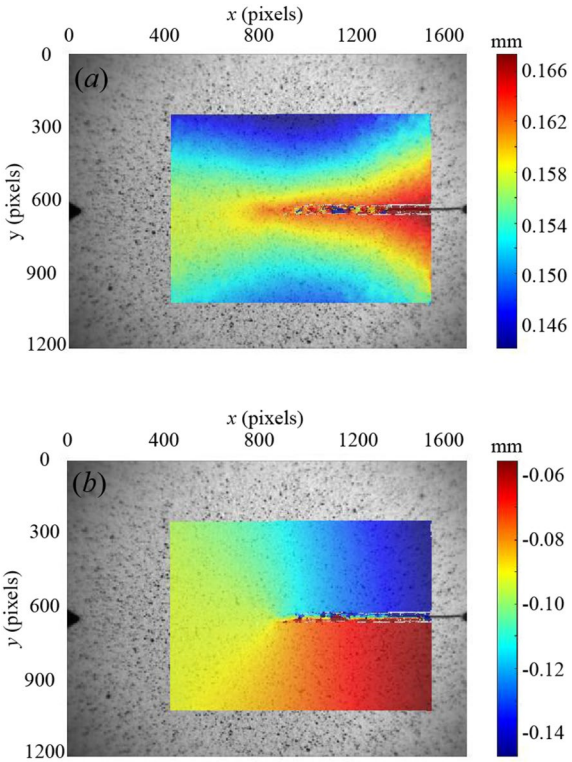

Figure 5 Displacement cloud at crack length a = 17.65 mm, P = 2400 N: **a** Displacement cloud in the Lateral direction (u); **b** displacement cloud in the vertical direction (v)

As already noted, the use of DIC to obtain the original displacement field data causes noise interference. One cause of this noise is the loss of DIC data when speckle analysis is performed with a specific step size and fitting area, the speckle at the crack boundary is destroyed and the corresponding displacement field data are missing, which leads to errors in determining the area of

Table 2 Mass fraction of chemical composition of U71MnG rail steel

C	Si	Mn	P	S	Cr	V	Al
0.65–0.76	0.15–0.58	0.70–1.20	<0.03	<0.025	–	–	<0.01

the plastic zone. Zhu et al. [36] combined DIC technology with the element-free Galerkin algorithm, and used DIC to derive these missing displacement field nodes required by a meshless numerical model. Ye and Wang [37] calculated the stress and displacement fields during the crack growth process based on a multi hidden layer BP neural network model. They compared the numerical solution with the experimental solution, and showed that their solution had high accuracy. The complete boundary displacement field data is the key to obtain the accurate experimental plastic zone and its trailing area, and the interpolated displacement field data is the key to obtain the accurate plastic zone area, so the displacement field data should be solved again by the corresponding method of the examination rate. In this study, a BP neural network was used to fit the displacement field. The gradient descent method is used to search for the best weight vector and threshold vector according to the loss function using the back propagation algorithm. Subsequently, the full-field displacement field was calculated. As shown in Figure 6(a), it gives the plastic zone at the crack tip with a pixel spacing of 9. The displacement field was fitted by the BP neural network to obtain a smooth and continuous displacement field. A plastic zone with a pixel spacing of 1 was obtained, as shown in Figure 6(b), which made the plastic zone more consistent with the experimental plasticity.

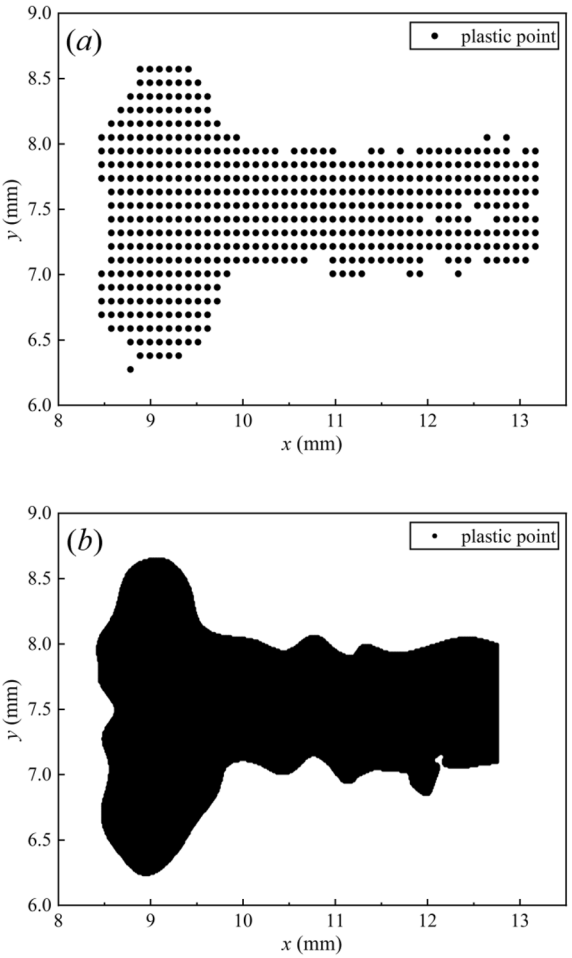

Figure 6 Plastic zone at the crack tip: **a** Crack tip plastic zone with a pixel spacing of 9; **b** crack tip plastic zone with a pixel spacing of 1

3.3 Levenberg-Marquardt (L-M) Algorithm Solution Parameters

The calculation of the stress intensity factor parameters is highly sensitive to the position of the crack tip and size of the calculation area. It is essential to accurate locate the position of the crack tip and outer diameter of the fitting area. Yang et al. [38] used the L-M algorithm to calculate the crack tip position, which was regarded as an unknown quantity. Relatively accurate positions and parameters of the crack tip were obtained. Zhou and Liu [39] deduced the relative error between the Westergaard model stress component σ_y and exact solution stress component σ^*_y in infinitely large plates. They observed that the error was small when the fitting outer diameter was 0.1 times of the crack length, a, and the plastic zone can be up to $0.2a$.

As shown in Figure 7, the crack length is 17.35 mm. The plastic field area is removed by taking the plastic zone boundary as the inner diameter, and the fitting outer diameter is 1.856 mm, which is approximately 0.1 times of the crack length and meets the accuracy requirements. The corresponding stress intensity factor is obtained using the parameters A, B, C, F, and ρ solved by L-M nonlinear iteration.

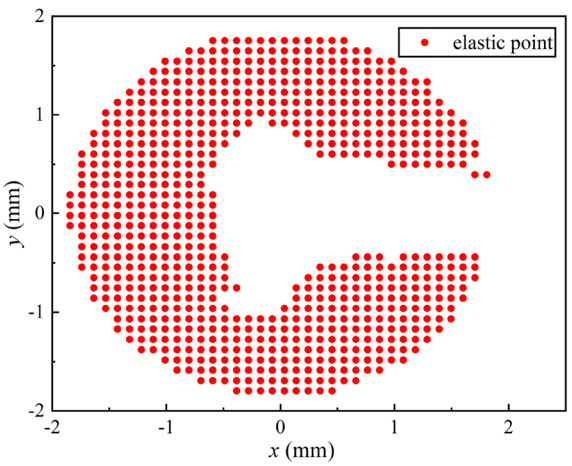

Figure 7 Elastic region used for crack tip parameter fitting

4 Results and Analysis

The displacement field data were obtained using DIC at $P = 2400$ N for various crack lengths and the experimental plastic zone was found. Parameters A, B, C, F, and ρ calculated from the elastic field data were used to obtain the theoretical plastic zone and compared with the plastic zone obtained by theoretical and experimental calculations of the CJP and modified CJP (CJP*) models. As shown in Figure 8, when the plastic zone is large in the later stage of crack growth, the theoretical plastic zone of the modified model and the CJP model is the same as the experimental plastic zone, which proves that the modified model describes the effect of the CJP model in the large plastic zone.

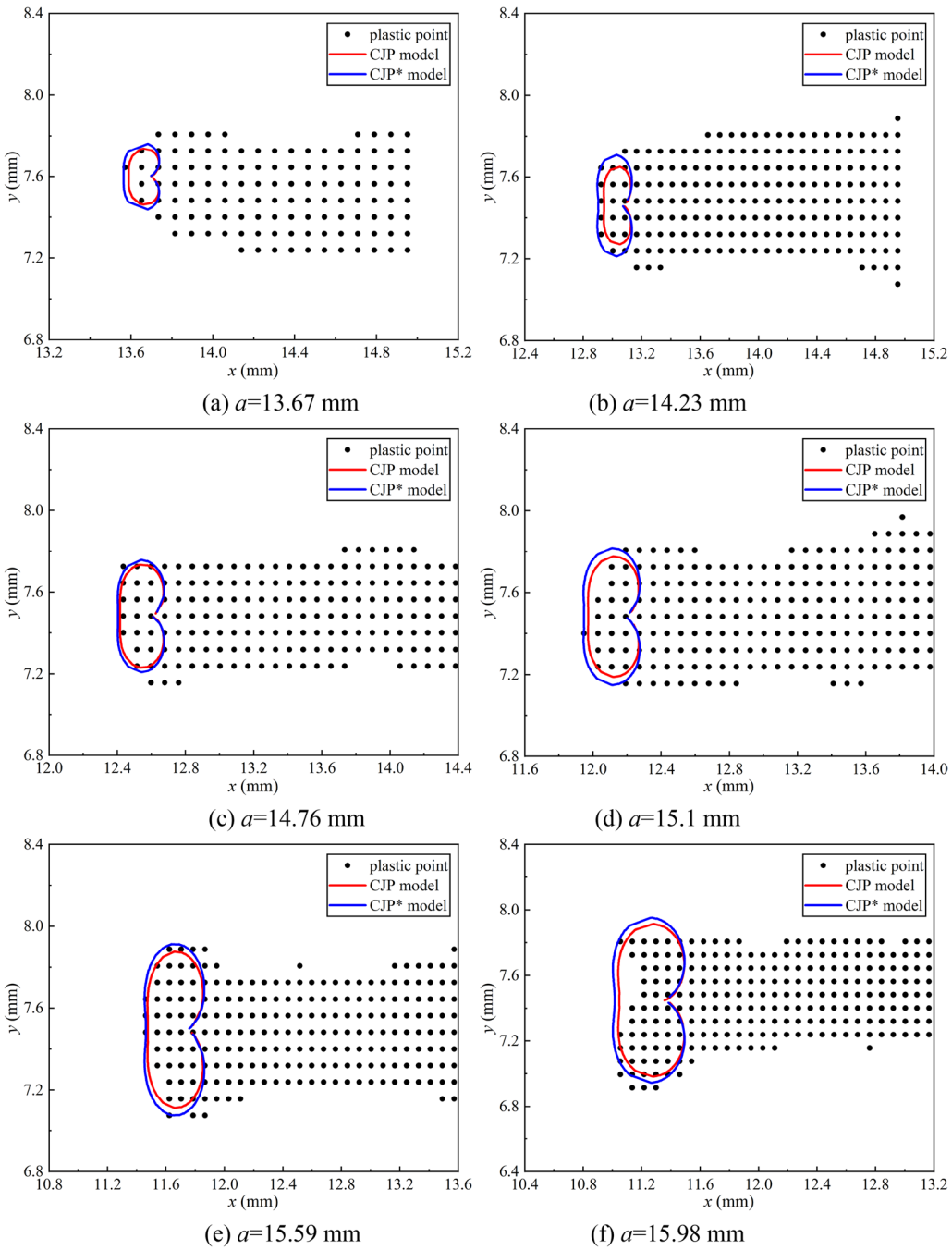

Figure 8 Comparison between the size of the experimental plastic zone and the predictions obtained by the modified CJP (CJP*) and CJP models

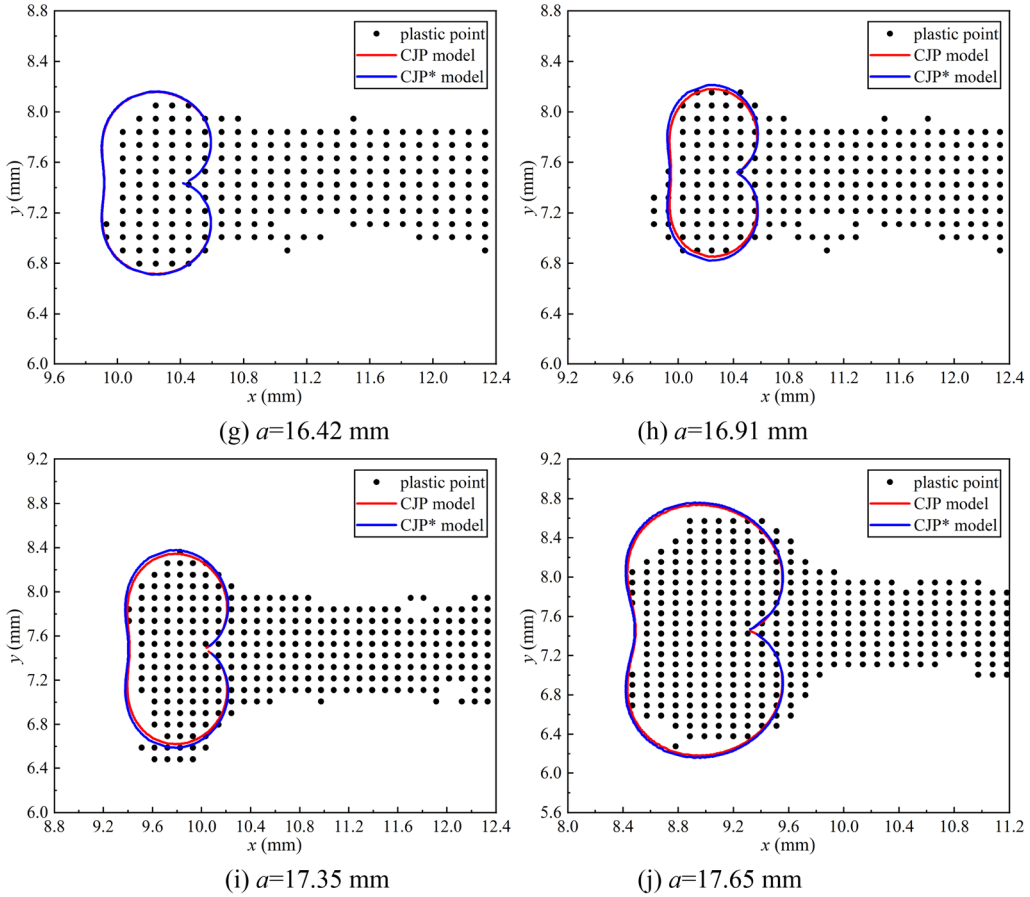

Figure 8 continued

However, when the plastic zone is small in the early stage of crack growth, the description of the modified model is better, but that of the CJP model is quite different. It can be seen from the comparison of the plastic zones that the dislocation correction model has a good effect in each stage of the crack, which compensates for the insufficiency of the CJP model with low plasticity and provides a more accurate basis for describing the plastic zone.

The area of the plastic zone is an important parameter for characterising crack growth rate, and a plastic zone with a pixel spacing of 1 (1 pixel is equal to 0.0114 mm) was obtained through the BP neural network. A rectangle with a fixed area of $l \times w$ mm^2 and a pixel spacing of 1 was used. The area $A_e = l \times w \times n/m$ mm^2 of the plastic zone is obtained by the correlation between the point and area in the rectangular region and in the plastic zone. n and m are the number of pixels of the plastic zone and the rectangle, respectively, and the relative error between the theoretical plastic zone and the experimental plastic zone is $e = (A_p - A_e)/A_e$ (%). The plastic zone area and relative error for each crack length are presented in Table 3.

In Table 3, when the crack length is greater than 16.42 mm, both models provide a good description of the plastic zone size with little difference between them. The modified model retains the advantages of the CJP model for the large-range elastic approximation of the crack-tip field. The modified model provides a better description when the plastic zone area is smaller, particularly in the early stages of crack growth. This is because the dislocation field corrects the displacement near the crack surface, which is different from plastic correction. The dislocation accumulation phenomenon was not evident when the plastic zone was small. The effect of crack-tip plasticity was small, and dislocation slip was dominant. A blunting parameter was introduced to ensure that the corrected model gave better results.

Figure 9 shows the change in the relative error of the two crack-tip models with the area of the experimental plastic zone. It clearly shows the error and trend of the modified and CJP models in the same experimental plastic zone. The change in the modified model was within ± 10%, whereas the CJP model had a larger error at low plasticity, with a maximum of approximately 37.8%.

Table 3 Experimental and theoretical plastic zone area and their relative error

a (mm)	Experimental (mm^2)	CJP (mm^2)	Error (%)	CJP* (mm^2)	Error (%)
13.67	0.04574647	0.033037	−27.78134	0.047273	3.33727
14.23	0.09682542	0.060300	−37.72283	0.098710	1.94593
14.76	0.12467664	0.107842	−13.50273	0.124361	−0.25346
15.1	0.18494582	0.146789	−20.63161	0.185198	0.13633
15.59	0.28605631	0.240395	−15.96244	0.285922	−0.04695
15.98	0.41793767	0.351728	−15.84190	0.413103	−1.15681
16.42	0.83251788	0.838024	0.66140	0.845276	1.53251
16.91	0.88106797	0.857363	−2.69046	0.918066	4.19925
17.35	1.29518556	1.262811	−2.49961	1.342719	3.66999
17.65	2.52213032	2.691615	6.71991	2.770852	9.86155

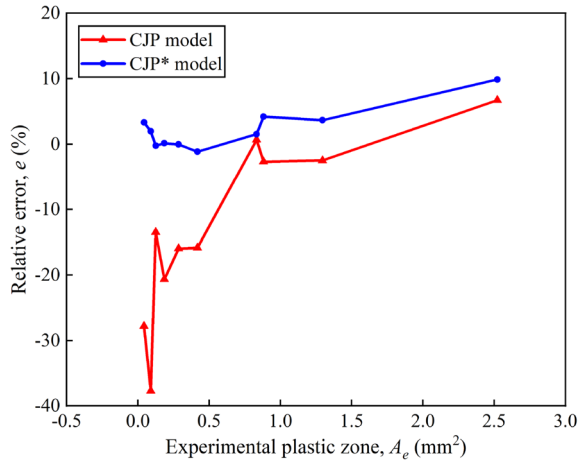

Figure 9 Relationship between relative error and experimental plastic zone area

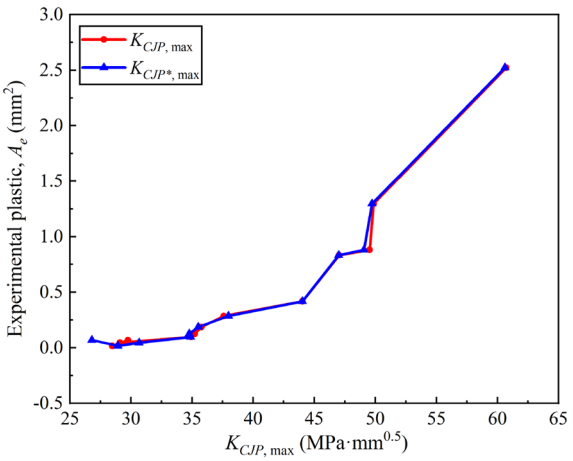

Figure 10 Relationship between the area of the experimental plastic zone and the stress intensity factors $K_{CJP,\ max}$ and $K_{CJP^*,\ max}$

There may be certain errors in calculation errors in this study, and there could be other factors that have not been considered, such as the hardening, roughness, and grain size of the material. Although the influencing factors of blunting were considered in this study, many other factors were not considered, and it was difficult to quantify these errors. However, the errors of other factors were consistent, and their variation and general trends also appear sensible.

As shown in Figure 10, the area of the plastic zone has an almost linear relationship with the stress intensity factor $K_{CJP,\ max}$, which can be expressed as a direct parameter for driving cracks, where $K_{CJP} = K_F - K_R$. When the plastic zone is small, the stress intensity factor $K_{CJP^*,\ max}$ of the modified model has evident stability and accuracy, and the curve is smoother, which proves that the effect of the modified model is better.

Figure 11 shows the changing trend in the stress intensity factors with the load when the crack length is 17.65 mm. For the same crack length, the stress intensity factor K_{CJP^*} of the modified model is almost the same as that of the CJP model. The stress intensity factor during unloading is larger under the same load. During the unloading process, the plastic zone has reversed plastic behaviour to form a cyclic plastic zone which has residual stress in the plastic zone. The larger the plastic zone, the larger the residual stress, and the stronger the ability to resist external load.

Compared with the differences in the stress intensity factors before and after correction under different loads, $K_{CJP} = K_F - K_R$ shows only a slight change, indicating that dislocation correction does not influence the plastic correction of the CJP model, which proves that the dislocation correction is correct. It is independent of plasticity-induced closure and elasto-plastic-compatible stresses. However, the dislocation field has a significant influence on *Ks*, the formation of which is a shear stress intensity factor caused by the

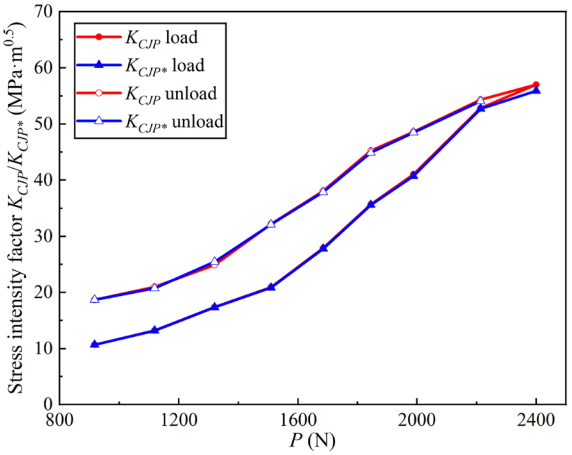

Figure 11 Variation trend of stress intensity factors K_{CJP} and K_{CJP*} with load

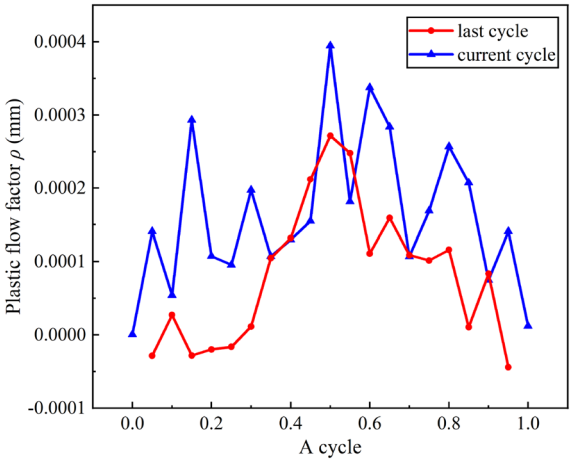

Figure 13 Variation trend of plastic flow factor ρ with load cycle

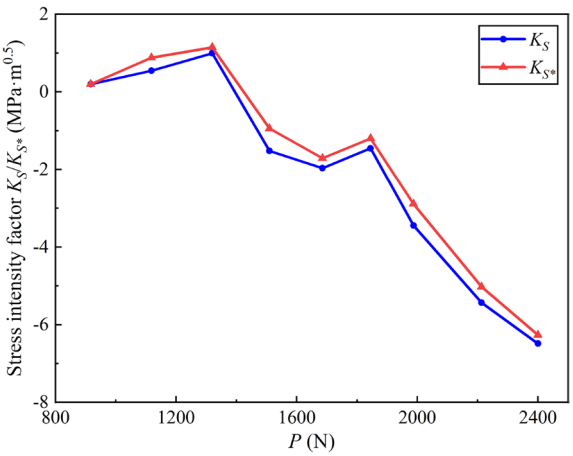

Figure 12 Variation trend of stress intensity factors K_S and K_{S*} with load

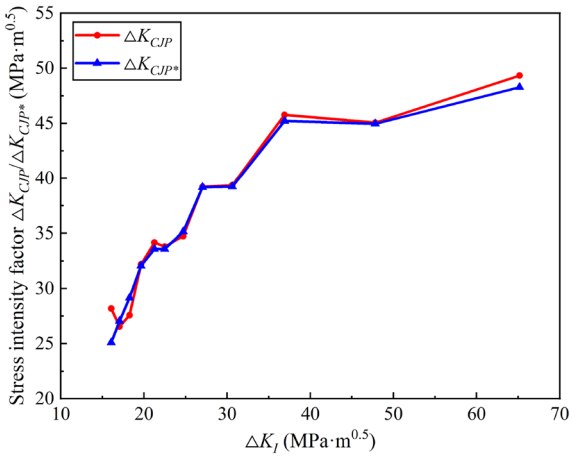

Figure 14 Variation trend of stress intensity factors ΔK_{CJP} and ΔK_{CJP*} with ΔK_I

elastoplastic compatibility stress at the elastic-plastic boundary along the crack wake. Its direction is x-positive when the crack is closed and x-negative when the crack is opened. The dislocation slip is due to the movement of dislocations towards the crack tip under the external load, and it is difficult to reverse after the dislocation slip occurs. The two forms exist independently, which causes K_{S*} to form a changing trend, as shown in Figure 12.

Figure 13 shows that the plastic flow factor ρ generated by dislocation changes with the load cycle, and ρ also represents the amount of blunting. It increases with the increase in external load. ρ is larger when the crack length is 17.65 mm than when it is 17.35 mm, under the same load, indicating that ρ increases with the stress intensity factor, and the crack tip blunting is more significant. Baptista et al. [21] showed that when $\theta = \pi$, the displacement y near the crack must also add a blunt amount, which is the same as the y-direction displacement expressed in this paper. It can be explained as the increase in the blunting of the crack tip with the external load.

Figure 14 shows the changing trend of ΔK_{CJP*} and ΔK_{CJP} with ΔK_I. The modified model and the CJP model indicate similar trends in the change. When the ΔK_I is smaller, the modified model shows better stability and accuracy, and ΔK_{CJP*} and ΔK_{CJP} have a certain cubic relationship with ΔK_I. There is a certain linear relationship even in the early stage of crack propagation. This relationship is useful for engineering applications. The accuracy and stability of the stress intensity factor at small plasticity period proves the effect of the dislocation correction.

Figure 15 shows the trend in the variation of the stress intensity factor with crack length a. In the initial stages of crack growth, ΔK_{CJP} obtained using the CJP model is larger than ΔK_I. It reflects the influence of shielding effects of the wake contact and elastoplastic compatible stress in the CJP model. The range of the stress intensity factor ΔK_{CJP^*}, of the modified model, shows better stability and accuracy. However, when the crack length is larger than 17.35 mm, ΔK_{CJP^*} is lower than the traditional stress intensity factor, indicating that the CJP model has an advantage when describing plastic-induced shielding. When the plastic zone is large, the residual stress reduces the stress intensity factor generated by the external load and reduces the crack growth rate.

5 Conclusions

(1) The CJP model was modified to account for crack blunting based on the crack tip dislocation field. The BP neural network algorithm was used to fit the experimental plastic zone to make it more continuous and crack tip elastic field data obtained by using DIC technology, and the stress intensity factors were calculated by using the L-M nonlinear algorithm. When the crack length was greater than 15.98 mm, the modified model maintained the description effect of the CJP model on the large plastic zone. The theoretical plastic zone was the same as the experimental plastic zone, with a maximum error of 9.86%. When the crack length is less than 15.98 mm, the corrected model shows better results, within ±10%, whereas the maximum error when using the CJP model is approximately 37.8%.

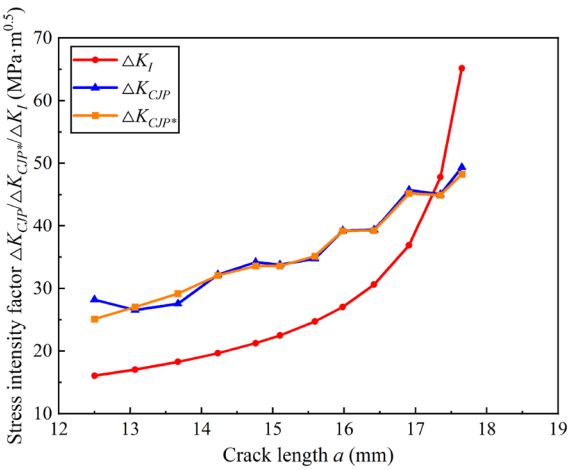

Figure 15 Variation trend of stress intensity factors ΔK_{CJP}, ΔK_{CJP^*} and ΔK_I with crack length a

(2) The stress intensity factor during unloading is larger under the same load. During the unloading process, the plastic zone is compressed, the plastic zone has reversed plastic behaviour to form a cyclic plastic zone which has residual stress in the plastic zone. The larger the plastic zone, the larger the residual stress, and the stronger the ability to resist external load.

(3) Under the action of an external load, the dislocation moves toward the crack tip; K_S points to the crack tip when the crack closes and deviates from the crack tip when the crack opens. Dislocation motion and plastic behaviour are two independent influencing factors that lead to a large change in K_S.

(4) The plastic flow factor ρ generated by the dislocation field increases with the external load. The value ρ is larger under the same load when the crack length is longer. It corrects the displacement of the crack surface as the amount of crack-tip blunting.

Acknowledgements
Not applicable.

Author contributions
BY was in charge of the whole trial; JL wrote the manuscript; JL and SW carried out the experimental analyses and the numerical simulations; SX, GY and TZ guided the experiments, BY and MJ revised the manuscript. All authors read and approved the final manuscript.

Authors' Information
Jian Li, born in 1998, is currently a master candidate at *State Key Laboratory of Traction Power, Southwest Jiaotong University, China*. His research interests include fracture mechanics and damage tolerance analysis.
Bing Yang, born in 1979, is currently a professor at *State Key Laboratory of Traction Power, Southwest Jiaotong University, China*. He received his PhD degree from *Southwest Jiaotong University, China*, in 2011. His research interests include strength of vehicle structure, and fatigue and fracture of materials.
Shuancheng Wang, born in 1994, is currently a PhD candidate at *State Key Laboratory of Traction Power, Southwest Jiaotong University, China*. His research interests include fatigue analysis and structural reliability.
M N James, born in 1953, is currently a professor at *School of Engineering, Computing & Mathematics, University of Plymouth, England*. He received his PhD degree from *University of Cambridge, England*, in 1983. His research interests include fatigue and fracture, structural integrity.
Shoune Xiao, born in 1964, is currently a professor at *State Key Laboratory of Traction Power, Southwest Jiaotong University, China*. He received his master degree from *Southwest Jiaotong University, China*, in 1988. His research interests include vehicle dynamics, collision, structural strength and fatigue reliability.
Tao Zhu, born in 1984, is currently an associate professor at *State Key Laboratory of Traction Power, Southwest Jiaotong University, China*. He received his PhD degree from *Southwest Jiaotong University, China*, in 2012. His research interests include, vehicle dynamics, collision.
Guangwu Yang, born in 1977, is currently a professor at *State Key Laboratory of Traction Power, Southwest Jiaotong University, China*. He received his PhD degree from *Southwest Jiaotong University, China*, in 2005. His research interests include vehicle dynamics, vibration, and fatigue reliability.

Funding
Supported by Sichuan Science and Technology Program of China (Grant No. 2022YFH0075), Opening Project of State Key Laboratory of Performance Monitoring and Protecting of Rail Transit Infrastructure of China (Grant No.

HJGZ2021113), Independent Research Project of State Key Laboratory of Traction Power of China (Grant No. 2022TPL_T13).

Data availability

The data that support the findings of this study will be available from the corresponding author upon reasonable request.

Competing interests

The authors declare no competing financial interests.

Received: 9 July 2022 Revised: 3 March 2023 Accepted: 9 March 2023
Published online: 06 April 2023

References

[1] M L Williams. On the stress distribution at the base of a stationary crack. *Journal of Applied Mechanics*, 1956, 24(1): 109-114.
[2] R J Sanford. A critical re-examination of the Westergaard method for solving opening-mode crack problems. *Mechanics Research Communications*, 1979, 6(5): 289-294.
[3] K Ramesh, S Gupta, A A Kelkar. Evaluation of stress field parameters in fracture mechanics by photoelasticity—Revisited. *Engineering Fracture Mechanics*, 1997, 56(1): 25-41.
[4] J R Yates, M Zanganeh, Y H Tai. Quantifying crack tip displacement fields with DIC. *Engineering Fracture Mechanics*, 2010, 77(11): 2063-2076.
[5] S Seitl, L Malikova, V Ruzicka, et al. Williams' expansion-based approximation of the displacement field in an Al 2024 compact tension specimen reconstructed from optical measurements. *Fatigue & Fracture of Engineering Materials & Structures*, 2018, 41(10): 2187-2196.
[6] X L Huang, Y H Liu, X B Huang. Analytical characterizations of crack tip plastic zone size for central-cracked unstiffened and stiffened plates under biaxial loading. *Engineering Fracture Mechanics*, 2019, 206: 1-20.
[7] G R Irwin. Analysis of stresses and strains near end of a crack traversing a plate. *Journal of Applied Mechanics*, 1956, 24(24): 361-364.
[8] D S Dugdale. Yielding of steel sheets containing slits. *Journal of the Mechanics and Physics of Solids*, 1960, 8(2): 100-104.
[9] W Elber. Fatigue crack closure under cyclic tension. *Engineering Fracture Mechanics*, 1970, 2(1): 37-45.
[10] B Budiansky, J W Hutchinson. Analysis of closure in fatigue crack growth. *Journal of Applied Mechanics*, 1978, 45(2): 267-276.
[11] K Tan, V Postel, Y J Liu, et al. Development of a photomicroscope method for in situ damage monitoring under ultrasonic fatigue test. *International Journal of Structural Integrity*, 2022, 13(2), 237-250.
[12] F A Díaz, J M Vasco-Olmo, E López-Alba, et al. Experimental evaluation of effective stress intensity factor using thermoelastic stress analysis and digital image correlation. *International Journal of Fatigue*, 2020, 135: 105567.
[13] Yang, Z J Wei, Z Liao, et al. Influence of single peak overload on crack closure effect of industrial pure titanium CT specimen. *Journal of Mechanical Engineering*, 2021, 57(12): 169-178. (in Chinese)
[14] C J Christopher, M N James, E A Patterson, et al. Towards a new model of crack tip stress fields. *International Journal of Fracture*, 2007, 148(4): 361-371.
[15] M N James, C J Christopher, Y Lu, et al. Local crack plasticity and its influences on the global elastic stress field. *International Journal of Fatigue*, 2013, 46: 4-15.
[16] R Pippan, F O Riemelmoser. Visualization of the plasticity-induced crack closure under plane strain conditions. *Engineering Fracture Mechanics*, 1998, 60(3): 315-322.
[17] J M Vasco-Olmo, F A Díaz, A Camacho-Reyes, et al. Experimental evaluation of plastic wake on growing fatigue cracks from the analysis of residual displacement fields. *Fatigue & Fracture of Engineering Materials & Structures*, 2022, 45(5): 1494-1504.
[18] A T Taddesse, S P Zhu, D Liao, et al. Cyclic plastic zone-based notch analysis and damage evolution model for fatigue life prediction of metals. *Materials and Design*, 2020, 191: 108639.
[19] J C He, S P Zhu, A T Taddesse, et al. Evaluation of critical distance, highly stressed volume, and weakest-link methods in notch fatigue analysis. *International Journal of Fracture*, 2022, 162: 106950.
[20] A T Taddesse, S P Zhu, D Liao, et al. Combined notch and size effects modeling of metallic materials for LCF using plasticity reformulated critical distance theory. *Journal of Materials Research and Technology*, 2022, 18: 470-484.
[21] J B Baptista, F V Antunes, L Correia, et al. A numerical study of the effect of single overloads on plasticity induced crack closure. *Theoretical and Applied Fracture Mechanics*, 2017, 88: 51-63.
[22] J Dundurs, T Mura. Interaction between an edge dislocation and a circular inclusion. *Journal of the Mechanics & Physics of Solids*, 1964, 12(3): 177-189.
[23] C Atkinson, M F Kanninen. A simple representation of crack tip plasticity: The inclined strip yield superdislocation model. *International Journal of Fracture*, 1977, 13(2): 151-163.
[24] S Pommier. Cyclic plasticity and variable amplitude fatigue. *International Journal of Fatigue*, 2003, 25(9): 983-997.
[25] S Pommier, R Hamam. Incremental model for fatigue crack growth based on a displacement partitioning hypothesis of mode I elastic–plastic displacement fields. *Fatigue & Fracture of Engineering Materials & Structures*, 2010, 30(7): 582-598.
[26] H Hamli-Benzahar. Theoretical analysis of image forces during the interaction between a dislocation and semi-infinite crack in bi-material. *Theoretical and Applied Fracture Mechanics*, 2021, 114: 103005.
[27] C He, X Li, Y J Liu, et al. Localized dislocation interactions within slip bands and crack initiation in Mg-10Gd-3Y-0.3Zr alloy. *International Journal of Fracture*, 2021, 150: 106302.
[28] B Yang, M N James. Fatigue crack growth rate curve and application method based on CJP model. *Journal of Mechanical Engineering*, 2018, 54(18): 76-84. (in Chinese)
[29] B Yang, J M Vasco-Olmo, F A Díaz, et al. A more effective rationalisation of fatigue crack growth rate data for various specimen geometries and stress ratios using the CJP model. *International Journal of Fatigue*, 2018, 114: 189-197.
[30] J R Barber. *Elasticity*. Dordrecht: Kluwer Academic Press, 1992.
[31] H F Bueckner. Novel principle for the computation of stress intensity factors. *Zeitschrift Fuer Angewandte Mathematik & Mechanik*, 1970, 50: 529-546.
[32] N I Muskhelishvili. *Some basic problems of the mathematical theory of elasticity*. Dordrecht: Noordhoff International Press, 1977.
[33] B Yang, Z J Wei, Z Liao, et al. Optimisation method for determination of crack tip position based on Gauss-Newton iterative technique. *Chinese Journal of Mechanical Engineering*, 2021, 34(2). https://doi.org/10.1186/s10033-021-00585-0
[34] F D Carolo, D Palumbo, R D Finis, et al. Investigation of the plastic zone around the crack tip in small-scale pure Titanium specimens by means of thermal signal analysis and digital image correlation. *IOP Conference Series: Materials Science and Engineering*, 2021, 1038(1): 012011.
[35] B Pan. Full-field strain measurement using a two-dimensional Savitzky-Golay digital differentiator in digital image correlation. *Optical Engineering*, 2007, 46(3): 033601.
[36] Z H Zhu, S H Luo, Q S Feng, et al. A hybrid DIC-EFG method for strain field characterization and stress intensity factor evaluation of a fatigue crack. *Measurement*, 2020, 154: 107498.
[37] W J Ye, L H Wang. Analysis of fatigue crack growth based on back propagation neural network. *Quarterly Journal of Mechanics*, 2021, 42(4): 752-762. (in Chinese)
[38] B Yang, Z J Wei, F A Díaz, et al. New algorithm for optimised fitting of DIC data to crack tip plastic zone using the CJP model. *Theoretical and Applied Fracture Mechanics*, 2021, 113(8): 102950.
[39] R Z Zhou, G T Liu. On the truncation error of the main term in the expansion of Williams complex characteristics. *Journal of Fuzhou University*, 1986, 2: 89-100. (in Chinese)